Reversible Laser-Induced Amplified Spontaneous Emission from Coexisting Tetragonal and Orthorhombic Phases in Hybrid Lead Halide Perovskites

*Fabian Panzer, Sebastian Baderschneider, Tanaji P. Gujar, Thomas Unger, Sergey Bagnich, Marius Jakoby, Heinz Bässler, Sven Hüttner, Jürgen Köhler, Ralf Moos, Mukundan Thelakkat, Richard Hildner, and Anna Köhler**

The photoluminescence in a lead halide perovskite is measured for different temperatures (5–300 K) and excitation fluences (21–1615 μJ cm^{-2}). It is found that amplified spontaneous emission (ASE) is observed for an excitation density larger than about 1×10^{18} cm^{-3} for both the tetragonal phase above 163 K and the orthorhombic phase below about 163 K. The fluence that is required to obtain this excitation density depends on temperature and phase since the nonradiative decay of excitations is temperature activated with different activation energies of 85 ± 20 and 24 ± 5 meV for the tetragonal and orthorhombic phase, respectively. The ASE from the tetragonal phase—usually prevailing at temperatures above about 163 K—can also be observed at 5 K, in addition to the ASE from the orthorhombic phase, when the sample is previously exposed to a fluence exceeding 630 μJ cm^{-2} at a photon energy of 3.68 eV. This additional ASE can be removed by mild heating to 35 K or optically, by exposing the sample by typically a few seconds with a fluence around 630 μJ cm^{-2}. The physical mechanism underlying this optically induced phase transition process is discussed. It is demonstrated that this phase change can, in principle, be used for an all-optical "write–read–erase" memory device.

1. Introduction

Organic–inorganic mixed halide perovskites received enormous attention over the last few years. They allow for the production of crystalline films with a high structural stability[1,2] and with low trap-state densities.[3] This enabled the fabrication of perovskites solar cells that convinced the solar cell community with high performances such as power conversion efficiencies of over 20%,[4,5] while offering the possibility for low cost production, e.g., by solution-processing.[6] Meanwhile, further device applications for organic–inorganic mixed halide perovskites have been discovered. For example, in 2014, low threshold levels for amplified spontaneous emission showed that mixed halide perovskites can also be used for the facile fabrication of lasers with high quality factors.[7–10] Furthermore, it is known that most halide perovskite materials can exist in different crystal structures, depending on environmental conditions such as temperature.[11–13] Here, we show that a coexistence of tetragonal and orthorhombic phases within apparently the same crystalline grain can be optically induced into the halide perovskite $CH_3NH_3PbI_3$ at low temperatures, leading to amplified spontaneous emission (ASE) simultaneously at two distinct wavelengths. The ASE feature associated with the (high temperature) tetragonal phase can be reproducibly written, read-out, and erased at 5 K by choosing appropriate

F. Panzer, T. Unger, Dr. S. Bagnich, M. Jakoby, Prof. A. Köhler
Experimental Physics II
University of Bayreuth
95440 Bayreuth, Germany
E-mail: anna.koehler@uni-bayreuth.de
F. Panzer, S. Baderschneider, T. Unger, Prof. H. Bässler, Prof. J. Köhler, Dr. R. Hildner, Prof. A. Köhler
Bayreuth Institute of Macromolecular Research (BIMF)
University of Bayreuth
95440 Bayreuth, Germany
F. Panzer, Prof. R. Moos
Department of Functional Materials
University of Bayreuth
95440 Bayreuth, Germany
S. Baderschneider, Prof. J. Köhler, Prof. R. Hildner
Experimental Physics IV
University of Bayreuth
95440 Bayreuth, Germany
Dr. T. P. Gujar, Prof. M. Thelakkat
Applied Functional Polymers
Macromolecular Chemistry I
University of Bayreuth
95440 Bayreuth, Germany
Prof. S. Hüttner
Organic and Hybrid Electronics
Macromolecular Chemistry I
University of Bayreuth
95440 Bayreuth, Germany

DOI: 10.1002/adom.201500765

laser fluences or raising the temperature. Finally, we show to which extend our findings can be exploited for use as an all optical data storage device.

The paper is structured as follows. Section 2 briefly introduces the spectral features observed in the photoluminescence spectra for excitation at low and at high fluence as a function of temperature. In Section 3 we show that ASE of the tetragonal phase—usually prevailing at temperatures above 163 K—can be observed at 5 K provided the sample was previously exposed to high intensity illumination, and this feature can be removed by mild heating or illumination at moderate intensity. We discuss the underlying physical mechanism. Section 4 demonstrates that this phenomenon could, in principle, be used toward an all-optical 2D "write–read–erase" random access memory device, though its technological exploitation is limited by the associated low (<35 K) operational temperature. Our findings are summarized in Section 5, and experimental details are detailed in Section 6.

2. Spectroscopic Characterization of the Emission

2.1. Results

We synthesized a pore free and compact crystalline $CH_3NH_3PbI_3$ layer consisting of micrometer sized grains by slightly modifying a published procedure.[14] To characterize the emission from this film, we carried out temperature dependent steady state photoluminescence (PL) measurements at different excitation fluences. Using a *low* excitation fluence of 0.75 μJ cm^{-2}, we observe the broad and featureless emission centered at about 1.60 eV at 300 K that is associated with the radiative decay of excited states in the tetragonal crystal structure (**Figure 1**a).[15,16] On cooling the sample to 140 K, a higher energy emission appears around 1.68 eV along with the existing emission at 1.57 eV. On further cooling to 40 K, the emission shifts to 1.64 eV and it dominates the spectrum. Upon excitation with a *higher* fluence of 85 μJ cm^{-2} we observe the same behavior of the broad and featureless emission bands upon cooling. However, in addition to these bands, sharp peaks emerge, and strongly grow in intensity, upon cooling (Figure 1b). Like the broad emission bands, the narrow peaks also show a red shift with decreasing temperature down to 1.61 eV at 5 K. For ease of reference, characteristic emissions obtained for low and high fluences are displayed on a linear scale in Figure 1c for a temperature of 170 and 40 K, respectively. The fluence dependence of the integrated photoluminescence intensity and of the full width at half maximum (FWHM) of the emission are displayed in **Figure 2**a,b for three different temperatures. The associated spectra are detailed in the Supporting Information (Figure S1). These data show a characteristic threshold behavior, and we find that t*he lower the temperature, the lower the value of the threshold fluence*. Vice versa, for the fluence of 85 μJ cm^{-2} chosen here, the threshold temperature for the narrow peak at 1.56 eV to appear is ≈210 K in case of the "high-temperature" regime, and for the "low-temperature" range the narrow peak at 1.65 eV appears below 135 K (see Figure 2c,d).

2.2. Discussion

The hybrid perovskite $CH_3NH_3PbI_3$ is well known to undergo a transition from the tetragonal to the orthorhombic structure at about 160 K.[12,13,17] Using X-ray diffraction (XRD), we confirmed that this transition also takes place in our sample (see Figure S2, Supporting Information). At low fluence such as 0.75 μJ cm^{-2}, we thus attribute the broad emission above 160 K centered at 1.60 to 1.75 eV to emission from the tetragonal crystal structure, while the broad emission centered at 1.64–1.68 eV at temperatures below 160 K is attributed to the orthorhombic phase. The narrow, intense peaks that appear in addition upon cooling when exciting at high fluence such as 85 μJ cm^{-2} are attributed ASE.[8,18,19] We base our assignment on the observation that, at a given temperature, these peaks show a characteristic line narrowing with simultaneous increase in emission intensity as a function of excitation fluence. This is summarized in Figure 2a,b and further detailed in the Supporting Information (Figure S1). For both the tetragonal and the orthorhombic phases, the emission shows a roughly linear bathochromic shift, consistent with earlier work,[13,20] and an increasing intensity upon cooling from 300 to 150 K (tetragonal) and from 140 to 5 K (orthorhombic).

To account for the intensity dependence of the emission at low fluence, we recall that the intensity of emission is given by $I(T) = \frac{k_r}{k_r + k_{nr}} I_0$, where I_0 is the emission intensity in the absence of nonradiative decay processes, k_r and k_{nr} denote the radiative and nonradiative decay rates. We measured the temperature-dependence of the absorption at the excitation wavelength and found it to be independent of temperature (Figure S3a, Supporting Information). The Einstein coefficients then require the radiative decay rate k_r also to be temperature-independent. Thus, any temperature dependence of the emission must be attributed to k_{nr}. This applies to both the tetragonal and the orthorhombic phase. If we consider a simple thermally activated nonradiative decay process and write $k_{nr} = k_{nr}^0 \, e^{-\frac{E_B}{kT}}$, the temperature-dependent emission intensity becomes $I(T) = [1 + \frac{k_{nr}^0}{k_r} \exp(-\frac{E_B}{kT})]^{-1} I_0$. Fitting the experimentally obtained temperature dependent PL intensity we find activation energies E_B of 85 ± 20 and 24 ± 5 meV for the temperature-dependent nonradiative decay rate in the tetragonal and orthorhombic phase, respectively. The temperature dependence of the absorption and of the emission as well as the associated fits is shown in Figure S3 of the Supporting Information. The straight lines that are obtained in an Arrhenius-like representation, where $\ln[\frac{I(0)}{I(T)} - 1]$ is displayed as a function of inverse temperature, confirm that a thermally activated nonradiative decay process is a valid approach.

A thermally activated nonradiative decay process is also the mechanism that can account for the temperature-dependent ASE. The evolution of ASE in both phases as a function of temperature at constant higher laser fluence is remarkable, and it is consistent with the observation that the minimum fluence required to induce the ASE reduces with temperature. A prerequisite for amplified spontaneous emission is that the

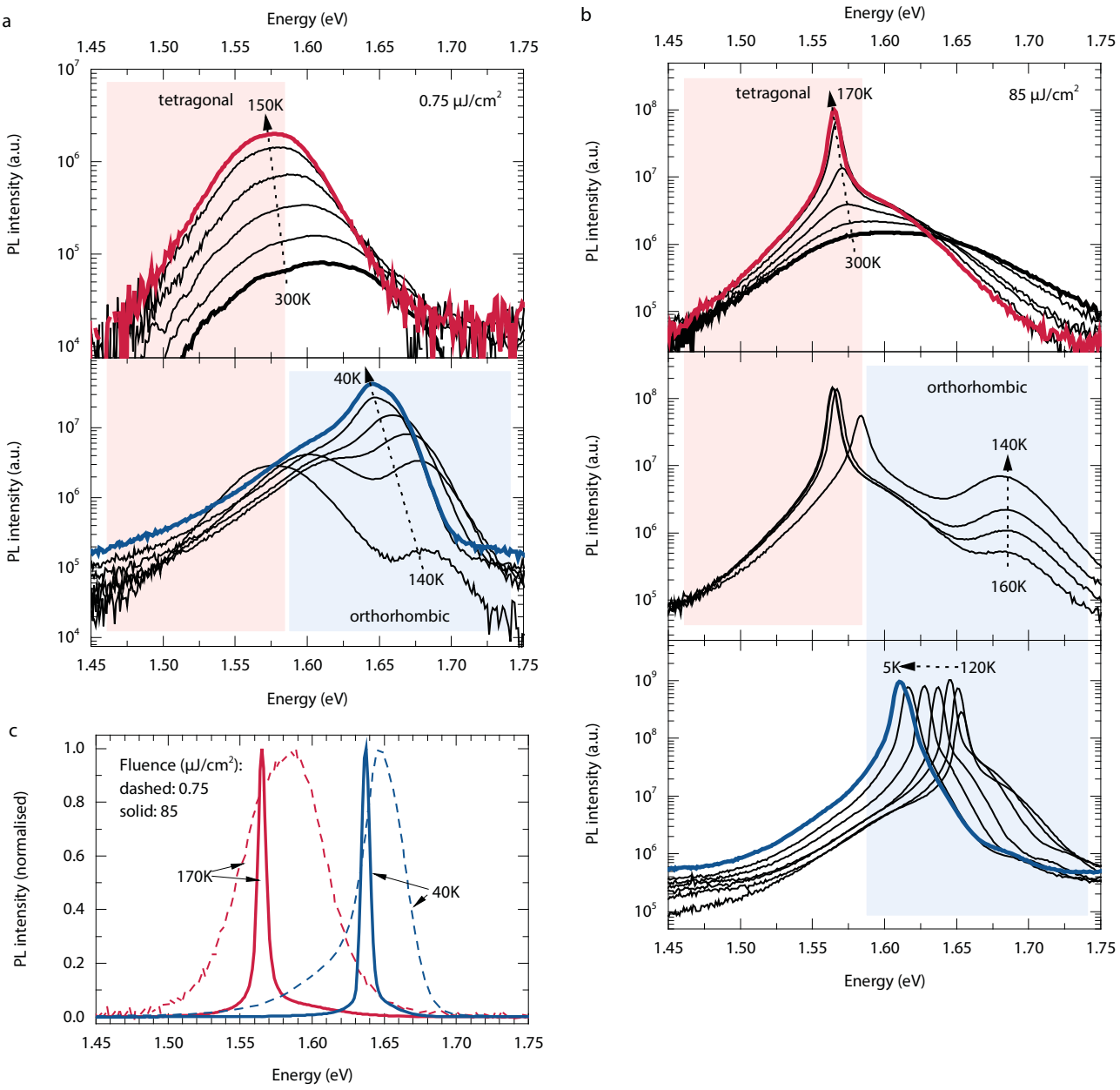

Figure 1. Temperature dependent photoluminescence (PL) spectra recorded with a) fluences of 0.75 μJ cm^{-2} and b) of 85 μJ cm^{-2}. The characteristic spectral ranges of tetragonal and orthorhombic PL are indicated by the red and blue areas, respectively. c) The characteristic PL spectra in the tetragonal phase at 170 K (red line) and in the orthorhombic phase at 40 K (blue line) for both high fluence (solid line) and low fluence (dashed line) on a linear scale.

optical gain exceeds the radiative and nonradiative losses in the medium. Thus it can only occur at a sufficiently high density of excitations. Such a density n builds up if the generation rate G, controlled by the fluence, exceeds the rates of radiative and nonradiative decay, i.e., $0 < \frac{dn}{dt} = G - (k_r + k_{nr}(T))n$. From the above-mentioned temperature-dependent absorption and photoluminescence measurements we found k_r and G to be temperature independent while k_{nr} shows a simple temperature-activated behavior with activation energies of 85 ± 20 and 24 ± 5 meV for the tetragonal and orthorhombic phases, respectively. By combining the fluence dependence and temperature dependence with the activation energy, we can *estimate the threshold exciton density n that is required for ASE* to take place in our sample. We obtain $n_{threshold}^{tetragonal} = (1.02 \pm 0.2)\ 10^{18}$ cm^{-3} for the tetragonal phase from 200 to 280 K and $n_{threshold}^{orthorhombic} = (1.4 \pm 0.2)\ 10^{18}$ cm^{-3} for the orthorhombic phase at 135 K. The fact that for both phases the threshold exciton density required for ASE is found within the same range and essentially independent of temperature is a gratifying confirmation of our approach (Figure 2e). The estimate is based on the notion that, at a certain temperature, the density of excitations, n, contributing to ASE is given by $n = n_{generated}\ \Phi = n_{generated} \frac{I(T)}{I_0}$, where Φ is the photoluminescence

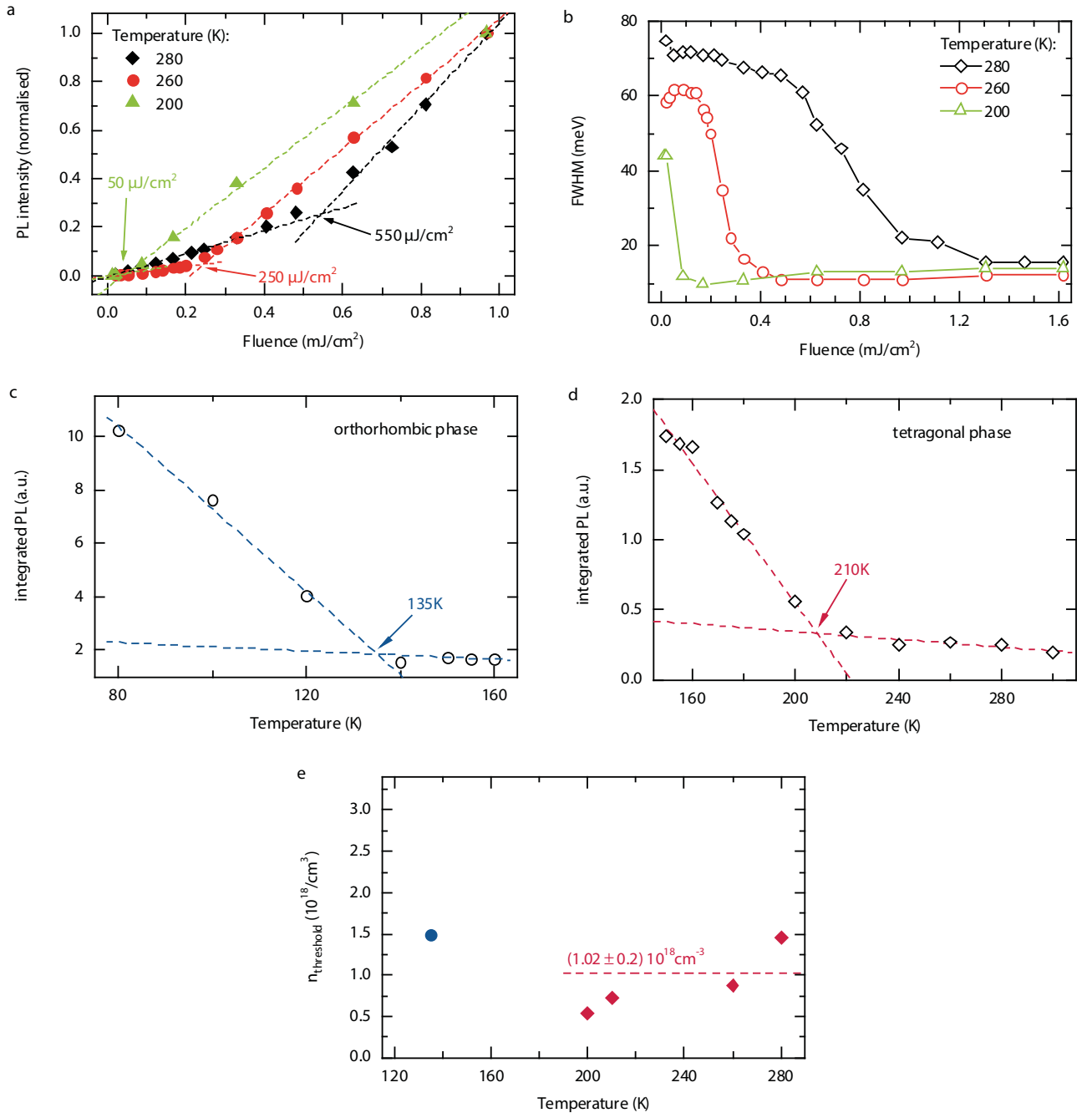

Figure 2. a) The integrated photoluminescence (PL) intensity and b) the full width at half maximum (FWHM) for excitation at 3.68 eV as a function of laser fluence from 21 to 1615 μJ cm^{-2} at 280, 260, and 200 K. c) The integrated PL intensity as a function of temperature, recorded with a laser fluence of 85 μJ cm^{-2} for the temperature range between 80 and 160 K, and d) for the temperature range between 160 and 300 K. e) The calculated values of $n_{threshold}$ as a function of temperature. The average value of $n_{threshold}$ between 280 and 200 K is indicated as dashed line. The blue circle indicates the data point obtained for the orthorhombic phase, the red diamonds pertain to data points in the tetragonal phase.

quantum yield and $n_{generated}$ is the number of excitons generated at the excitation intensity in the excitation volume. $\frac{I(T)}{I_0}$ is given by $[1+\frac{k_{nr}^0}{k_r}\exp(-\frac{E_B}{kT})]^{-1}$. $n_{generated}$ is given by the excitation energy divided by the photon energy and excitation volume. When the threshold energy for ASE is used for the excitation energy, this delivers the threshold density of excitations required for ASE. Full details of the calculation are given in the Supporting Information (Figure S4).

An essential notion in our discussion is the experimental finding that the nonradiative decay rate is thermally activated. From our data, we cannot unambiguously determine the origin of this thermally activated nonradiative decay process and its identification is not required for the analysis of our results.

Following the approach by Wu et al.,[15] Chen et al.,[21] and Savenije et al.,[22] one might attribute the nonradiative decay channel mainly to thermally activated dissociation of excitons and associate the activation energies with exciton binding energies. The values of 85 ± 20 and 24 ± 5 meV that we obtained for the tetragonal and orthorhombic phase are consistent with exciton binding energies reported earlier on the basis of temperature-dependent photoluminescence measurements.[15,22] We note, however, that exciton binding energies are known to vary within a rather broad range between few meV up to 70 meV,[13,15,22–27] and depend on the method chosen for investigation as well as on the particular crystal structure and composition of the hybrid perovskite.[27]

3. Reversible Induced Amplified Spontaneous Emission

3.1. Results

We observe that the emission recorded under low fluence excitation is different when the sample had previously been exposed to high fluence excitation. **Figure 3**a shows the photoluminescence taken from the sample at 5 K upon low fluence excitation at 21 μJ cm^{-2} before and after a previous exposure to 100 pulses at 15 Hz at a high fluence of 1615 μJ cm^{-2}. Even though the excitation fluence is as low as 21 μJ cm^{-2}, the emission centered at 1.61 eV at 5 K is narrow with a FWHM of 9 meV, implying that it is due to ASE from the orthorhombic phase. When the sample had previously been exposed to high fluence excitation, a second narrow low energy peak at 1.53 eV appears (FWHM of 9 meV) at the expense of intensity from the peak at 1.61 eV. The relative intensity of the two peaks can be controlled by tuning the preceding fluence. Figure 3b illustrates, on a logarithmic intensity scale, that the narrow low energy peak does not appear when previously exposing the sample to 100 pulses at 15 Hz with fluences of 168 or 329 μJ cm^{-2} and then recording the spectrum with excitation at 21 μJ cm^{-2}. When the sample is exposed to a previous pulse train with a fluence of 627 μJ cm^{-2}, the spectrum recorded under excitation at 21 μJ cm^{-2} shows a weak shoulder to appear at about 1.54 eV. For previous exposure to a pulse train with a fluence of 968, 1304 or 1615 μJ cm^{-2}, the spectra obtained with excitation at 21 μJ cm^{-2} clearly show a narrow low energy peak, centered at 1.530, 1.523, and 1.522 eV, respectively. While the intensity of the 1.61 eV peak is not affected by previous exposure at fluences of 168 or 329 μJ cm^{-2}, it reduces for previous exposure to fluences from 627 μJ cm^{-2} onward, whereas the intensity of the low energy shoulder or peak increases.

This narrow low energy peak that can be induced by previous exposure to fluences above 627 μJ cm^{-2} appears to be

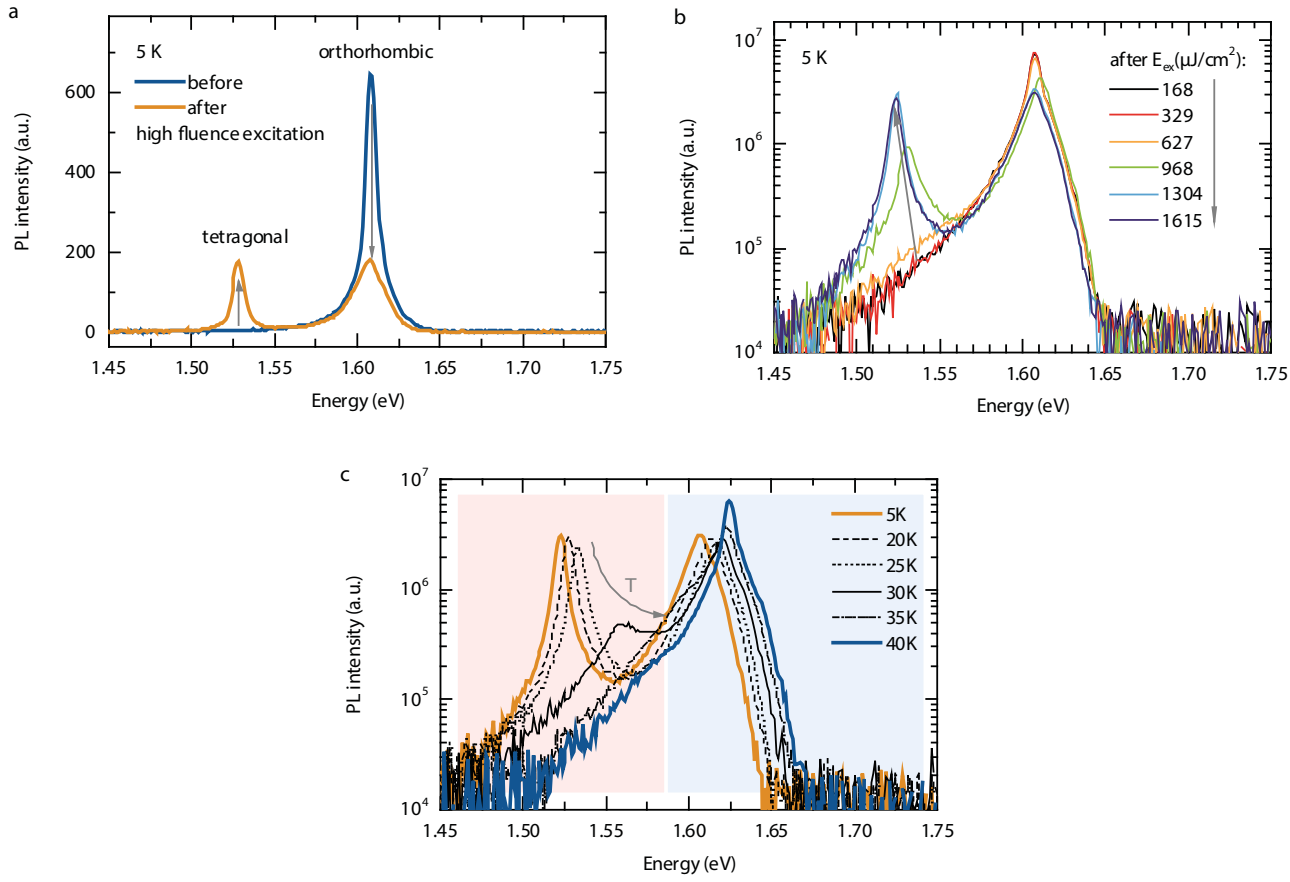

Figure 3. a) The emission spectrum of perovskite film at 5 K before (blue line) and after (orange line) high fluence (1615 μJ cm^{-2}) excitation, recorded with a fluence of 21 μJ cm^{-2}. b) Emission spectra recorded at low-excitation fluence (21 μJ cm^{-2}) after exposure to different high-fluence excitation. c) PL spectra for increasing temperatures, recorded with a fluence of 21 μJ cm^{-2} after previous exposure to 1615 μJ cm^{-2}.

stable with time when recorded using an excitation fluence of 21 μJ cm^{-2}. We observed no change in intensity in the course of our measurements. This is displayed in Figure S5 of the Supporting Information for a time scale of 30 min. Although the induced peak is stable with respect to time when recorded under low fluence, it is not stable with respect to temperature. Figure 3c shows that upon heating the sample from 5 K onward, the narrow low energy peak reduces in intensity and, concomitantly, shifts to higher energies. For temperatures above 35 K it disappears. Modeling the reduction in the low energy peak as a thermally activated process, using $\frac{\Delta I}{I_0} = e^{\frac{-\Delta E}{k_B T}}$, with ΔI being the change of emission intensity of the tetragonal phase relative to its maximum intensity I_0 at 5 K, yields a thermal activation energy of $\Delta E = 3$ meV for the removal of the narrow low energy peak.

In order to understand how exposure to high fluence may induce a remaining narrow low energy peak, it is instructive to consider the PL spectra recorded *during* exposure to high fluence. **Figure 4**a shows the emission spectra recorded for, first, exposure to a pulse train of 100 pulses at 15 Hz at a fluence of 329 μJ cm^{-2} (dashed line) and then recorded for exposure to the same pulse train at a fluence of 1615 μJ cm^{-2} (solid line). For reference, a Gaussian peak centered on 1.53 eV with a FWHM of 9 meV is also shown. Note that the spectra are displayed on a logarithmic intensity scale. In addition to the emission centered on 1.61 eV that is attributed to ASE from the orthorhombic phase, the spectrum recorded under a fluence of 1615 μJ cm^{-2} shows an emission band of unusual shape that ranges from about 1.58 to 1.53 eV, where its emission intensity falls off drastically. This low energy edge of the band perfectly matches the Gaussian peak centered on 1.53 eV with a FWHM of 9 meV. Figure 4b displays the spectra that result when the sample was *first* exposed to a pulse train of 100 pulses at 15 Hz at a fluence of 1615 μJ cm^{-2} and *then* recorded using a *single pulse* of increasing fluences from 168 μJ cm^{-2} onward. It is evident that the low energy edge of the additional band remains identical in all spectra, whereas the high energy edge of the band increases in energy with increasing fluence. The position of the maximum intensity in the band, close to the high energy edge, is displayed in Figure 4c as a function of fluence.

Further insight into the origin of the low energy band observed *during* high fluence excitation, and, concomitantly, the low energy peak seen *after* high fluence excitation can be

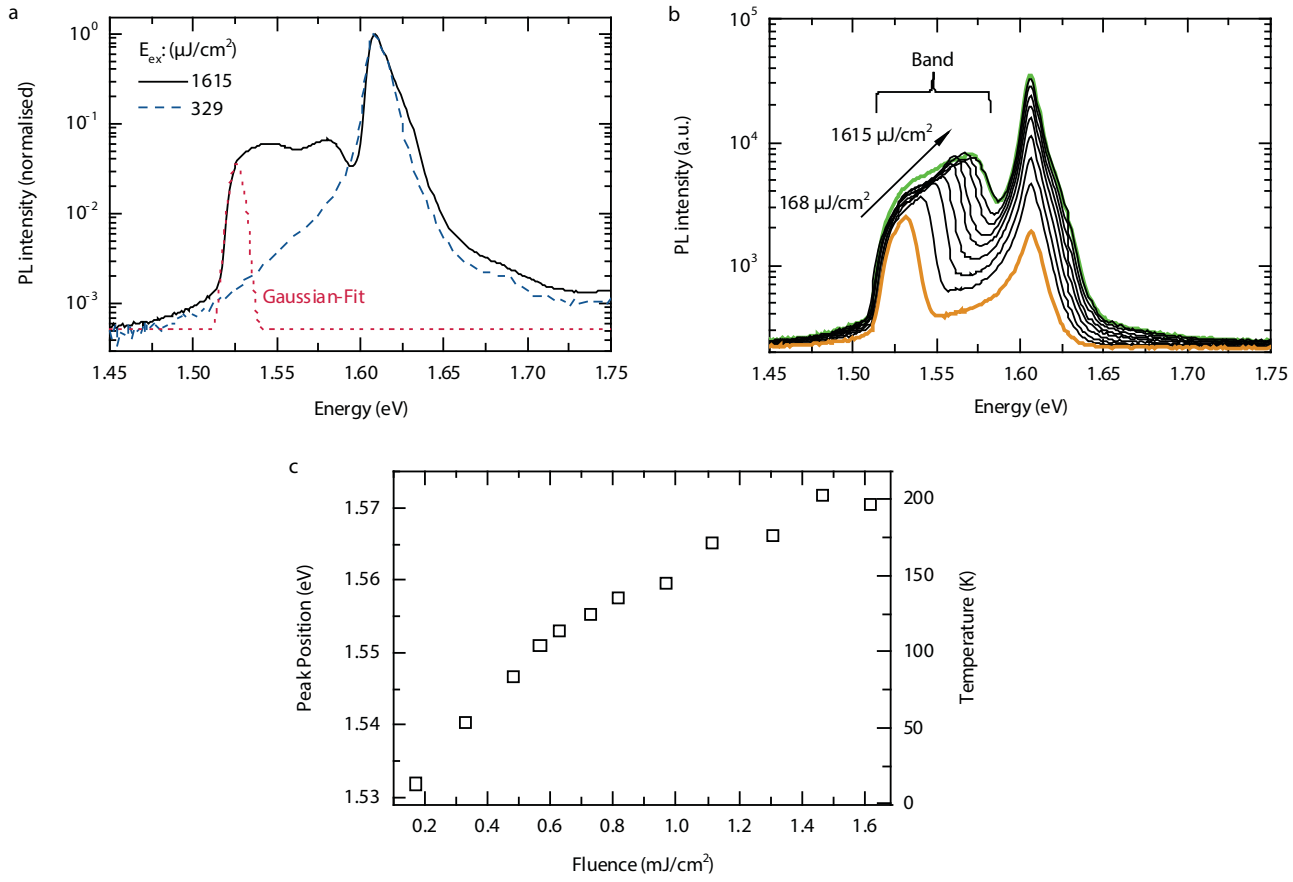

Figure 4. a) Emission spectra at 5 K recorded first using a low excitation fluence of 329 μJ cm^{-2} (dashed blue line) and then using a high excitation fluence of 1615 μJ cm^{-2} (solid black line). The red dotted line indicates a Gaussian peak with a full width at half maximum of 9 meV, corresponding to the value for the 5 K ASE of the tetragonal peak. b) Emission recorded with different high fluence excitation as indicated in the figure, after the sample was previously excited by a pulse train with fluences of 1615 μJ cm^{-2}. c) Energetic peak position of the peak in the lower energy band of (b), as a function of fluence. For ease of reference, the right axis shows the temperature associated with the peak position, taken from the dashed black line in Figure 6b below.

gained from time-resolved PL spectra (**Figure 5**). In Figure 5a, a film at 5 K had first been exposed to an excitation fluence of 1615 μJ cm^{-2}. After that, its emission was recorded at 5 K as a function of time for excitation at a fluence of 630 μJ cm^{-2} with 15 Hz. The top panel shows the resulting emission spectra on a linear scale at 0.1, 1.0, and 3.5 s after excitation. For all three spectra, the ASE peak of the orthorhombic phase at 1.61 eV is clearly visible. In addition, there is a low energy emission band with a peak that shifts from 1.55 eV to higher energies with increasing time. From about 1.0 s onward, it reduces in intensity while the 1.61 eV peak increases. This is displayed more clearly in the right panel. Similar spectra have been taken for a range of recording fluences, in each case after a previous exposure to a pulse train at 1615 μJ cm^{-2}. The peak position of the low energy band as a function of time is shown in Figure 5b for the different recording fluences. We observe two trends. First, the initial position of the low energy peak is at higher energies for higher fluences. Second, with increasing recording fluence the blue shift in peak position with time increases. While the low energy peak remains essentially constant at about 1.532 eV upon recording at 168 μJ cm^{-2}, it shifts by about 20 meV to higher energies within less than a second when recording the spectra at 810 μJ cm^{-2}.

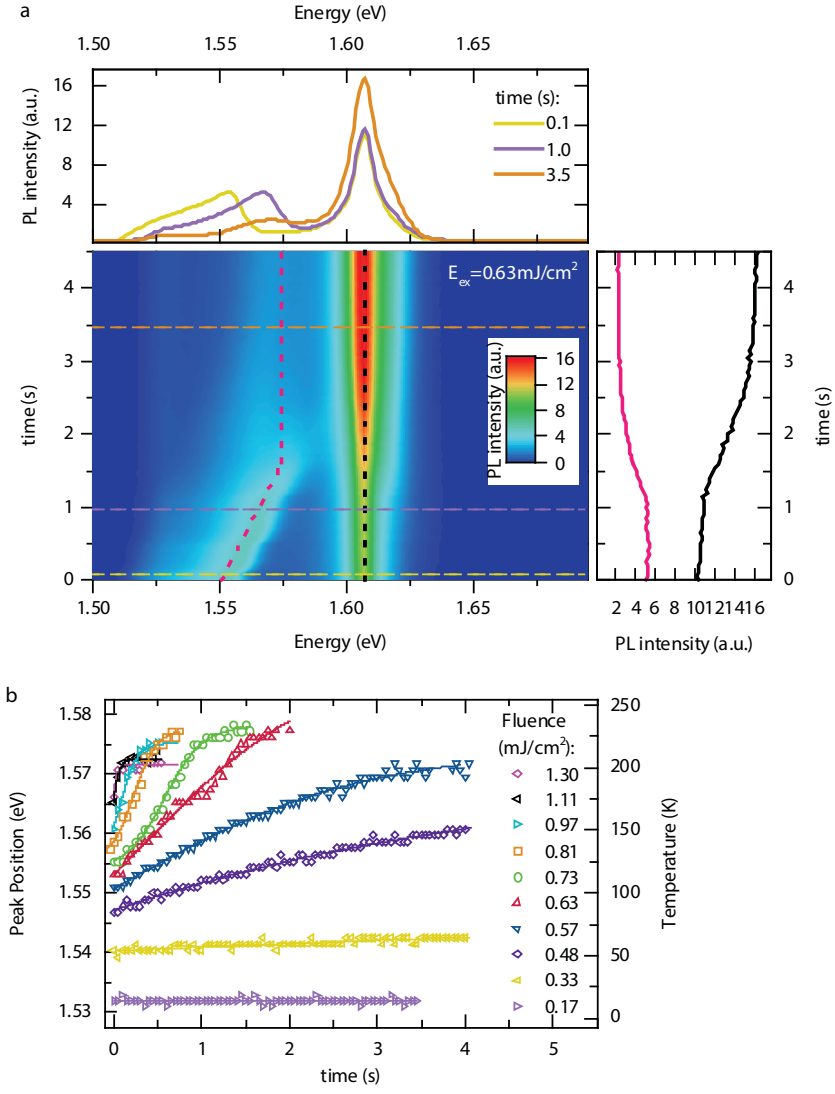

Figure 5. a) Emission spectra taken during illumination with a fluence of 630 μJ cm^{-2} as a function of time. The spectra are recorded immediately after the start of excitation. The film had previously been illuminated with high fluence of 1615 μJ cm^{-2}. The color indicates the photoluminescence intensity. The top panel shows the spectra on a linear scale, obtained after a time of 0.1 s (yellow line), 1.0 s (purple line), and 3.5 s (orange line). The right panel shows the PL intensity of the peak at 1.61 eV (black line), attributed to the orthorhombic phase, and of the peak in the low energy band (pink line), attributed to the tetragonal phase, as a function of time. Dashed lines in the central panel indicate these positions. b) The time-dependent evolution of the ASE peak in the tetragonal phase taken during illumination with a fluence as indicated in the figure. The sample had previously been illuminated with a high fluence of 1615 μJ cm^{-2}.

3.2. Discussion

The observation that a narrow low energy peak can be induced in a hybrid lead iodide perovskite by previous illumination at sufficiently high fluences, and that it can be removed by raising the temperature of the sample in a moderate way (Figure 3) raises some questions. First, it needs to be clarified what the narrow low energy emission is due to. Second, the process of how it forms and disappears for various experimental conditions (Figures 4 and 5) should be illuminated.

Various works have shown that the emission spectra of hybrid lead iodide perovskites can consist of different spectral features at low temperatures.[8,15,16,28,29] Xing et al.,[8] Fang et al.,[16] and Kong et al.[28] attribute the additional emission features they found in addition to the free exciton emission of the orthorhombic phase to the transition of bound excitons. Their feature is typically at about 40 meV below the energy of the free exciton transition and it has a spectral width in the range of 50 meV with PL lifetimes in the μs range.[16] In contrast to this, the low energy peak we observe, for example, in Figure 3a at 1.53 eV, is separated by about 80 meV from the emission feature of the orthorhombic phase and shows a FWHM of 9 meV. Time resolved PL measurements at low temperature using a STREAK Camera Setup further reveals, that the induced emission feature decays on a ns timescale (see Figure S6, Supporting Information). Due to these differences in spectral signature and dynamics we dismiss emission from the bound excitons as a possible explanation for the low energy peak. In a similar way, we also discard emission from trap states as a possible origin. Trap states were found to show a broadly distributed emission over a spectral range between approximately 1.3 and 1.5 eV, in contrast to the narrow emission we observe.[30] As will be shown in Section 4 further below, the narrow low energy

peak is highly reproducible and reversible, so that any permanent damage to the sample such as a decomposition of the organic cation can be excluded. An indication to the origin of the low energy peak is its narrow spectral width, e.g., of 9 meV at 1.53 eV (Figure 3a). This is in good agreement with the linewidth of about 10–15 meV that we found for the ASE peak from the tetragonal phase as shown in Figures 2b. In fact, the energies at which the laser-induced narrow low energy peak is observed matches with the energies where ASE from excitations in the tetragonal phase could be expected at low temperatures, provided that a linear extrapolation of the temperature dependence of the ASE peaks is valid as a first rough approximation. **Figure 6**b shows the temperature evolution of the ASE peaks in the orthorhombic and tetragonal phases, taken from Figure 1, along with the energies of the laser induced narrow low energy peak taken from Figure 3. Based on the narrow linewidth and energetic position we attribute the low energy emission to ASE from the tetragonal phase.

This assignment raises further questions. First of all, it is unexpected to observe a coexistence of peaks from the orthogonal and tetragonal phase below 40 K. Naively, one would expect energy transfer from the higher-energy peak to the induced lower-energy peak to suppress any emission from the orthorhombic phase. Evidently, the experimental data suggest that complete energy transfer does not occur, implying a somewhat localized character of the fast decaying excitations. Second, it is equally unexpected to observe emission from a *tetragonal* phase at temperatures as low as 5 K, since this phase is known to be the stable phase only above 160 K.

To account for the laser-induced existence of a tetragonal phase at low temperatures such as 5 K, we propose the following: *Local heating during excitation with high fluence induces a partial modification of the crystal structure toward the tetragonal phase.* This structure is then kinetically frozen in when the high intensity laser is turned off, thus leading to tetragonal inclusions in an orthorhombic matrix. Indeed, a simple estimate of the local heating effects during excitation indicates that a temperature above 163 K is reached for laser fluences above approximately 600 μJ cm^{-2}. This is in good agreement with the observation that a threshold fluence above about 630 μJ cm^{-2} is required to induce the 1.53 eV peak (see Figure 3b). Furthermore, based on the heat capacities and thermal conductivities of the lead halide perovskite and the supporting quartz substrate,[31] a fast drop of temperature back to 5 K can be expected on a timescale of a few 100 ns. The estimates for laser-induced heating and thermal dissipation of heat are detailed in the Supporting Information. Thus, the scenario of a remaining, kinetically frozen out tetragonal phase within an orthorhombic matrix is consistent with the material parameters. This hypothesis is illustrated in Figure 6a. Since the orthorhombic phase prevails at 5 K while the tetragonal phase is observed from 163 K onward, we consider that the two phases, pertaining to different configuration coordinates, are separated by an associated thermal activation energy of 163 K*k_B = 14 meV for the orthorhombic-to-tetragonal phase transition. From the analysis of Figure 3b we learned that a small activation energy of 3 meV is sufficient to convert the tetragonal phase back to the orthorhombic phase. This small activation energy for overcoming the barrier to the energetically more stable orthorhombic phase is reasonable given that the structural difference between the tetragonal and orthorhombic phase are only minor (lattice parameters: $a = c = 8.65$ Å, $b = 12.45$ Å at 155 K – tetragonal; $a = 8.90$ Å, $b = 12.67$ Å, $c = 8.65$ Å at 150 K – orthorhombic).[11] This picture also explains why coexisting emission from the tetragonal and orthorhombic phase has so far been reported only close to the temperature of the phase transition (≈160 K).[28]

Our hypothesis of local laser-induced heating is also consistent with the peculiar photoluminescence spectrum that is obtained *during* the high fluence (1615 μJ cm^{-2}) illumination, shown in Figure 4a. In this framework, we attribute the broad emission band to a superposition of ASEs from the tetragonal phase. Since the overall sample is held at 5 K, yet illumination with 1615 μJ cm^{-2} induces a local temperature well above 163 K, we expect a temperature gradient across the Gaussian excitation profile, resulting in ASEs from tetragonal phases with a temperature distribution. From the already obtained correlation

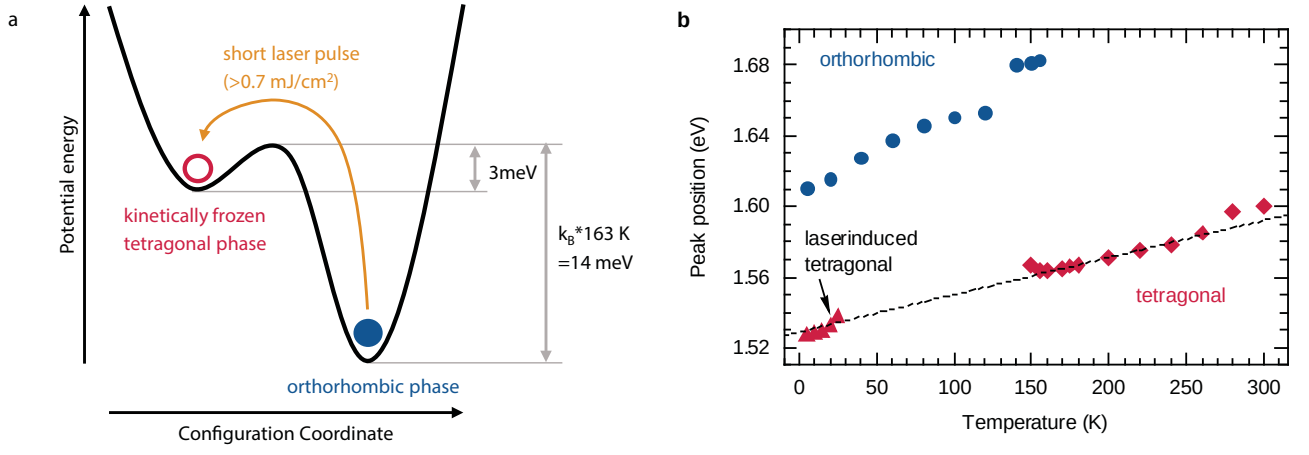

Figure 6. a) Schematic illustrating how illumination by an intense laser pulse can induce the formation of a metastable trapped tetragonal phase. b) The positions of the ASE peaks in the orthorhombic (blue dots) and in the tetragonal phase (red diamonds) as a function of temperature, recorded with a fluence of 85 μJ cm^{-2}. The dashed line indicates a linear interpolation of the peak position for the tetragonal phase. Red triangles indicate peak positions of ASE due to the tetragonal phase below 35 K that has been induced using previous illumination with a high fluence of 1615 μJ cm^{-2}.

between temperature and peak position of the ASE from the tetragonal phase (Figure 6b), the spectral positions can directly be transferred to corresponding temperatures. It is a gratifying consistency that the range of the band from 1.52 to 1.58 eV matches with a temperature range from 5 to 210 K.

This is further supported by Figure 4b. We consider that the preceding pulse train with 1615 μJ cm^{-2} induces the transition to the tetragonal phase that is then kinetically frozen in. For subsequent illumination with a low fluence pulse of 21 μJ cm^{-2}, we obtain the spectrum of ASE in the tetragonal phase at 5 K, i.e., a peak at 1.53 eV. Upon raising the fluence of the recording pulse from 168 μJ cm^{-2} onward, the center of the excitation spot raises in temperature, implying a temperature gradient to the border of the excitation spot. Consequently, the high energy tail of the band shifts to increasingly higher energies with temperature, while the low energy edge at 1.53 eV remains.

The energetic position of the high energy edge of the band in Figure 4b is displayed at the time $t = 0$ in Figure 5b. The shift that is observed in Figure 5 in the course of time when the spectrum is recorded during continuous illumination with 15 Hz at different fluences can easily be accounted for in our interpretation in a framework of local heating. It seems that for illumination with a low fluence, such as 168 μJ cm^{-2}, the heat deposited into the excitation spot with each pulse is dissipated sufficiently rapid so that both the temperature of the excited spot as well as that of the surrounding material at 5 K remain unaltered. For a higher fluence, e.g., 630 μJ cm^{-2}, the blue-shift of high-energy edge of the band within the first second indicates ASE from a tetragonal phase with an increasingly hot center, while the temperature surrounding the excitation spot is still sufficiently cold, i.e., below 35 K, to prevent an annealing of kinetically trapped tetragonal phase. This is also confirmed by the unaltered intensity of the ASE peak of the orthogonal phase at 1.61 eV. After about one second, a stationary position of the high energy edge in the ASE band from the tetragonal phase indicates a stationary equilibrium between the heat deposited into the excitation spot and the heat dissipated into the surrounding material, i.e., perovskite and substrate. Ultimately, this also raises the temperature of the material around the excitation spot beyond the 35 K limit, thus allowing for detrapping of the kinetically trapped tetragonal-to-orthorhombic phase transition. Accordingly, this is accompanied by an increase in the intensity of the ASE from the orthogonal phase at 1.61 eV.

The fact that the phase transitions between tetragonal and orthorhombic phase can be induced and removed by suitable adjusting the fluence of the laser illumination implies that lead halide perovskites could, in principle, be used to build an all-optical "random-access memory device."

4. All Optical Write–Read–Erase Cycles

4.1. Results

Figure 7 shows a simple proof-of-principle demonstration for such an all-optical memory device. As indicated in the top panel, the sample was illuminated with consecutive trains of 100 pulses at 15 Hz at, first, 1615 μJ cm^{-2} (the "write" process), then 21 μJ cm^{-2} (the "read" process), then 811 μJ cm^{-2} (the "erase" process) and finally again 21 μJ cm^{-2} (the "write" process). The intensities of the ASE peaks from the orthorhombic phase at 1.61 eV and of the tetragonal phase at 1.53 eV, recorded during the "read" process, are displayed in the bottom panel of Figure 7. The reproducibility of the process is clearly evident (see also Figure S5b, Supporting Information). After each "write" process, the intensities of the two ASE peaks are comparable, and after each "erase" process, the orthorhombic ASE peak takes a maximum value while the tetragonal ASE peak almost disappears. Due to the apparently localized character of the excitations associated with the ASE peaks, data writing and reading (i.e., a strong tetragonal ASE peak) can be implemented in a two-dimensional fashion.

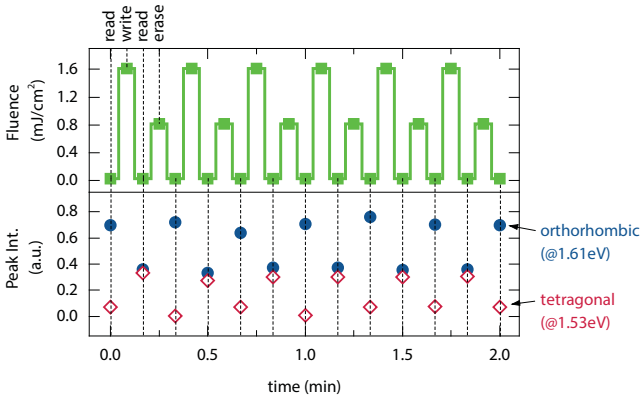

Figure 7. (Lower panel) Peak intensities at 5 K of the ASE at 1.61 eV (blue dots) in the orthorhombic phase and of the ASE at 1.53 eV (red diamonds), attributed to the tetragonal phase. The peak intensities were recorded using a fluence of 21 μJ cm^{-2} (= "read" mode) after previous illumination with pulses at a fluence of 1615 μJ cm^{-2} (= "write" mode) or at 811 μJ cm^{-2} (= "erase" mode) as illustrated in the upper panel.

The reproducibility of the "write" and "erase" processes is also manifested on a microscopic scale. **Figure 8** shows 2D intensity maps of the emission spectra for a 5 μm × 5 μm area of the film that was acquired at 1.5 K using a home-built confocal microscope with a spatial resolution of about 500 nm. The color scale decodes overall emission intensity that is spectrally integrated from 1.3 to 1.7 eV. The PL spectra, averaged over the entire 5 μm × 5 μm area for Figure 8a,c, and averaged over two smaller, 0.3 μm × 0.3 μm areas for Figure 8b, are shown in the bottom panels. In a pristine sample, only the 1.61 eV peak for the ASE of the orthorhombic phase is observed, though its intensity strongly varies across this area, as also observed by de Quilettes et al.[32] The size of the bright and darker regions in the film matches well with the grain size distribution found by transmission electron microscopy (0.2–1.2 μm), see Figure S7 in the Supporting Information.

After a "write" process, we observe first a change in intensity distribution across the sample area. Second, we observe that the additional 1.53 eV peak, indicative of a tetragonal crystal structure, has been induced everywhere across the investigated area (Figure 8b), albeit to different degrees. This observation suggests that both phases coexist within the same crystalline grain. Sample areas which have lower overall emission intensity have a higher relative contribution from the 1.53 eV peak. After an "erase" process, the original intensity distribution recovers and

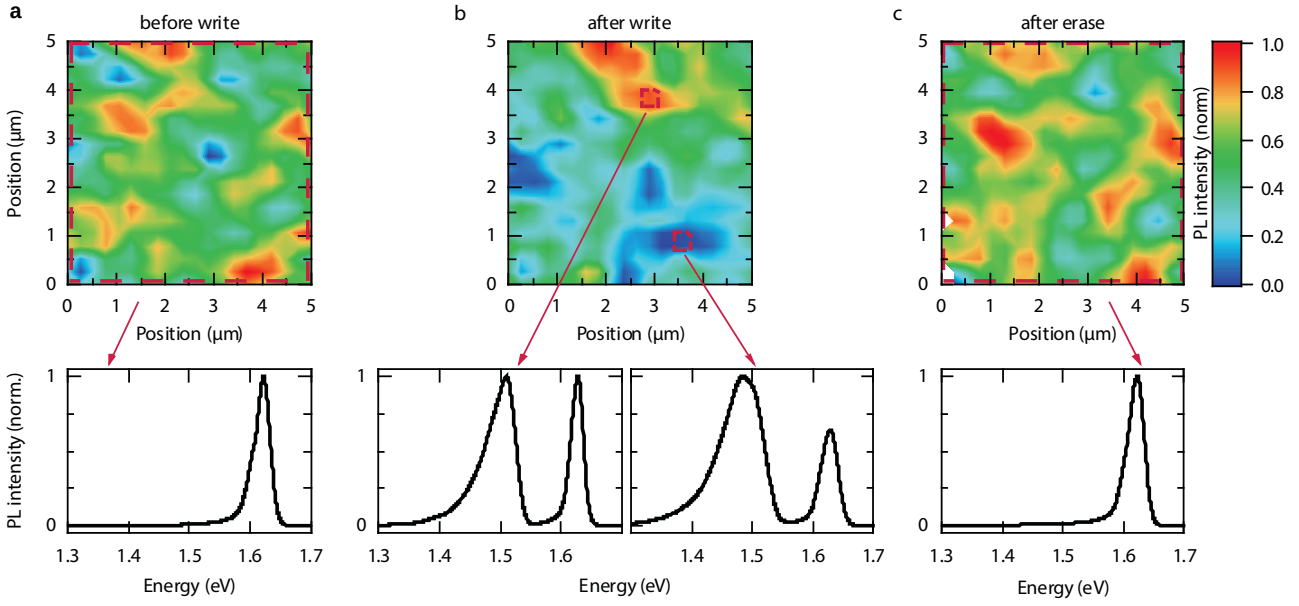

Figure 8. Spatially resolved emission map of the perovskite film at 1.5 K. a) 5×5 μm² area of the film before writing. The spectrally integrated PL intensity is color-coded (top panel). The PL spectrum averaged over the entire 5×5 μm² area demonstrates the presence of only the orthorhombic phase (bottom panel). b) The same 5×5 μm² area as in (a) after exposure to a high-fluence writing pulse (top panel). Two representative spectra acquired in the red boxed regions are depicted in the two bottom panels, indicating the presence of both the tetragonal as well as the orthorhombic phase all over the film. c) Same area after applying an erase pulse train (top panel) together with the PL spectrum integrated over the entire area (bottom panel), which shows that only the orthorhombic phase prevails.

we again observe merely emission at 1.61 eV across the entire sample area.

4.2. Discussion

The write–read–erase cycles shown in Figure 7 clearly demonstrate that, in principle, the phase transition in the lead halide perovskite could be used for "all optical random-access-memory" applications, using the induced tetragonal ASE peak as information carrier. The fluences used in Figure 7 for the "read" and for the "erase" process were chosen such as to ensure that the sample is not affected by the laser fluence during the "read" process, and to allow for a reasonably fast "erase" process. The "write" and the "read" process can be carried out in single shot mode, so that the time required for these processes is only limited by the pulse width of the laser and its repetition rate (see Figure S8, Supporting Information). The "erase" process, in contrast, requires sample heating above 35 K in an area surrounding the spot size. In the present mode of operation, this is achieved by controlling the balance of dose accumulation and heat dissipation. The initial laser energy is deposited in the excitation area through optical absorption followed by subsequent vibrational cooling, and the resulting heat flow into the surrounding material generates a temperature gradient. The "erase" process, i.e., the tetragonal-to-orthorhombic transition occurs for the sample area where the temperature is above 35 K yet below 160 K. An "erase" process with high fluence generates a strong temperature gradient across the excitation spot, so that the relevant temperature range is reached after a short accumulation time, yet only for a small circumference around the hotter center, leading to only partial "erase" of the 1.53 eV peak. A more complete "erase" process, requiring a shallower temperature gradient, can be obtained by using a moderate fluence over a longer period of time. This trade-off explains why, in this mode of optical excitation with visible light, a single-shot "erase" process is not possible. The situation may be different for excitation with light in the infra-red spectral range. An interesting feature is the option to "write" and "read" in a 2D fashion. The entire area could, in principle, be "written in" in parallel by using patterning and be "read out" by full size illumination combined with a charge-coupled device (CCD) camera, thus allowing for fast data access.

5. Concluding Summary

We have shown that for this lead halide perovskite amplified spontaneous emission occurs for an excitation density exceeding 1×10^{18} cm^{-3}. Whether this excitation density can be sustained depends on the balance between excitation fluence and sample temperature. At temperatures below the tetragonal-to-orthorhombic phase transition temperature of 163 K, high intensity laser pulses can locally heat the excitation spot thus resulting in a local orthorhombic-to-tetragonal phase transition that can get trapped kinetically if the surrounding material is at a temperature below 35 K. Detrapping is possible by mild heating above 35 K. This temperature can also be reached in the material surrounding the excitation spot by suitably adjusting the illumination fluence and time. In principle, this phase change could be employed to make an all optical

write–read–erase memory device, yet in practice the low temperature associated with the phase change limits its potential.

6. Experimental Section

Materials: All materials were purchased from Sigma-Aldrich and used as received.

CH_3NH_3I Synthesis: Methylammonium iodide (MAI) was synthesized as discussed elsewhere.[33] In short, MAI was synthesized by reacting 24 mL of methylamine (33 wt% in absolute ethanol) and 10 mL of hydroiodic acid (57 wt% in water) in a round-bottom flask at 0 °C for 2 h with stirring. The precipitate was recovered by putting the solution on a rotary evaporator and carefully removing the solvents at 50 °C. The white raw product MAI was redissolved in 80 mL absolute ethanol and precipitated with the addition diethyl ether. After filtration, the step was repeated two times and white solid was collected and dried at 60 °C in a vacuum oven for 24 h.

$CH_3NH_3PbI_3$ Film Preparation: The quartz substrates were cleaned with detergent diluted in deionized water, rinsed with deionized water, acetone, and ethanol, and dried with clean dry air. After cleaning, the substrates were transferred in a glovebox under nitrogen atmosphere. For perovskite formation, PbI_2 (1 M) was dissolved in *N,N*-dimethyl formamide overnight under stirring conditions at 100 °C and 80 µL solution was spin coated on the quartz substrates at 2000 rpm for 50 s, and dried at 100 °C for 5 min. Powder of MAI (100 mg) was spread out around the PbI_2 coated substrates with a petri dish covering on the top and heated at 165 °C for 13 h. To avoid that the samples were affected by air and humidity, 40 mg mL^{-1} poly(methylmethacrylate) (PMMA; Aldrich) in butyl acetate was spin-coated on top of the perovskite at 2000 rpm for 30 s. All steps were carried out under a nitrogen atmosphere in a glove box. See Figure S7 of the Supporting Information for morphology of the perovskite film showing the micrometer sized crystalline grains.

Temperature Dependent Emission Measurements: Emission spectra were recorded with a home-built setup. For cooling, the sample was put into a continuous flow cryostat (Oxford Instruments, Optistat CF) and excited by a Nitrogen Laser (LTB, MNL 100) with 337 nm pulses and a repetition rate of 15 Hz. Changes in the laser output energy were achieved by a controllable polarization attenuator, which led to available fluences in the range between 0.75 and 1615 µL cm^{-2}. The generated laser pulses were coupled into an optical fibre and directed toward the sample while being refocused by a lens. Emission from the sample was collected by another lens, focused to a spectrograph (Andor Shamrock 303i, spectral resolution ≈2 nm) which was coupled with a cooled CCD camera (Andor iDus), acting as the detection unit. Measured spectra were corrected for CCD and grating responsivity.

Spatially Resolved Emission Measurements: For the spatially resolved PL spectroscopy, we used a home-built low-temperature confocal microscope. The sample is mounted in a liquid-helium bath cryostat at 1.5 K. To read out the ASE from the perovskite films, we used a diode laser (BCL-020-405, CrystaLaser) operating at 405 nm. This laser light was directed to the cryostat, and focused by a microscope objective (NA = 0.85, Microthek) that was immersed in liquid helium. The combination of a motorized scan mirror and a telecentric lens system in front of the objective allowed to move the focal spot laterally across the sample in well-defined steps. The PL was collected by the same objective and passed the beam splitter and dielectric long pass filters to suppress residual laser light. Finally, it was focussed onto the entrance slit of a spectrograph (SpectraPro-150, Acton Research Corporation), spectrally dispersed by a grating (150 lines mm^{-1}), and imaged onto a CCD-camera (Pixelfly, PCO).

Supporting Information

The Supporting Information is available from the Wiley Online Library or from the author.

Acknowledgements

The authors acknowledge financial support by the Bavarian State Ministry of Science, Research, and the Arts through the Collaborative Research Network "Solar Technologies go Hybrid" and by the German Science Foundation DFG through the research training group GRK1640 and SFB 840. R.H. and S.B. acknowledge additional funding from DFG within project HI1508/2. The authors thank Cheng Li for stimulating discussions and Konstantin Schötz and Anna Gräser for the help with the setups.

Received: December 20, 2015
Revised: February 1, 2016
Published online: March 2, 2016

[1] H. S. Kim, C. R. Lee, J. H. Im, K. B. Lee, T. Moehl, A. Marchioro, S. J. Moon, R. Humphry-Baker, J. H. Yum, J. E. Moser, M. Grätzel, N. G. Park, *Sci. Rep.* **2012**, *2*, 591.
[2] J. Burschka, N. Pellet, S. J. Moon, R. Humphry-Baker, P. Gao, M. K. Nazeeruddin, M. Grätzel, *Nature* **2013**, *499*, 316.
[3] D. Shi, V. Adinolfi, R. Comin, M. Yuan, E. Alarousu, A. Buin, Y. Chen, S. Hoogland, A. Rothenberger, K. Katsiev, Y. Losovyj, X. Zhang, P. A. Dowben, O. F. Mohammed, E. H. Sargent, O. M. Bakr, *Science* **2015**, *347*, 519.
[4] NREL Solar efficiency chart, http://www.nrel.gov/ncpv/images/efficiency_chart.jpg (accessed: September **2015**).
[5] W. S. Yang, J. H. Noh, N. J. Jeon, Y. C. Kim, S. Ryu, J. Seo, S. I. Seok, *Science* **2015**, *348*, 1234.
[6] W. Nie, H. Tsai, R. Asadpour, J.-C. Blancon, A. J. Neukirch, G. Gupta, J. J. Crochet, M. Chhowalla, S. Tretiak, M. A. Alam, H.-L. Wang, A. D. Mohite, *Science* **2015**, *347*, 522.
[7] H. Zhu, Y. Fu, F. Meng, X. Wu, Z. Gong, Q. Ding, M. V. Gustafsson, M. T. Trinh, S. Jin, X. Y. Zhu, *Nat. Mater.* **2015**, *14*, 636.
[8] G. Xing, N. Mathews, S. S. Lim, N. Yantara, X. Liu, D. Sabba, M. Gratzel, S. Mhaisalkar, T. C. Sum, *Nat. Mater.* **2014**, *13*, 476.
[9] F. Deschler, M. Price, S. Pathak, L. E. Klintberg, D.-D. Jarausch, R. Higler, S. Hüttner, T. Leijtens, S. D. Stranks, H. J. Snaith, M. Atatüre, R. T. Phillips, R. H. Friend, *J. Phys. Chem. Lett.* **2014**, *5*, 1421.
[10] F. Laquai, *Nat. Mater.* **2014**, *13*, 429.
[11] T. Baikie, Y. Fang, J. M. Kadro, M. Schreyer, F. Wei, S. G. Mhaisalkar, M. Graetzel, T. J. White, *J. Mater. Chem. A* **2013**, *1*, 5628.
[12] C. C. Stoumpos, C. D. Malliakas, M. G. Kanatzidis, *Inorg. Chem.* **2013**, *52*, 9019.
[13] V. D'Innocenzo, G. Grancini, M. J. Alcocer, A. R. Kandada, S. D. Stranks, M. M. Lee, G. Lanzani, H. J. Snaith, A. Petrozza, *Nat. Commun.* **2014**, *5*, 3586.
[14] H. Zhou, Q. Chen, G. Li, S. Luo, T. B. Song, H. Duan, Z. Hong, J. You, Y. Liu, Y. Yang, *Science* **2014**, *345*, 542.
[15] K. Wu, A. Bera, C. Ma, Y. Du, Y. Yang, L. Li, T. Wu, *Phys. Chem. Chem. Phys.* **2014**, *16*, 22476.
[16] H.-H. Fang, R. Raissa, M. Abdu-Aguye, S. Adjokatse, G. R. Blake, J. Even, M. A. Loi, *Adv. Funct.Mater.* **2015**, *25*, 2378.
[17] J. Even, L. Pedesseau, C. Katan, M. Kepenekian, J.-S. Lauret, D. Sapori, E. Deleporte, *J. Phys. Chem. C* **2015**, *119*, 10161.
[18] B. R. Sutherland, S. Hoogland, M. M. Adachi, C. T. Wong, E. H. Sargent, *ACS Nano* **2014**, *8*, 10947.
[19] S. D. Stranks, S. M. Wood, K. Wojciechowski, F. Deschler, M. Saliba, H. Khandelwal, J. B. Patel, S. J. Elston, L. M. Herz, M. B. Johnston, A. P. Schenning, M. G. Debije, M. K. Riede, S. M. Morris, H. J. Snaith, *Nano Lett.* **2015**, *15*, 4935.
[20] R. Pässler, *Phys. Status Solidi B* **1997**, *200*, 155.
[21] K. Chen, A. J. Barker, F. L. C. Morgan, J. E. Halpert, J. M. Hodgkiss, *J. Phys. Chem. Lett.* **2015**, *6*, 153.

[22] T. J. Savenije, C. S. Ponseca, L. Kunneman, M. Abdellah, K. Zheng, Y. Tian, Q. Zhu, S. E. Canton, I. G. Scheblykin, T. Pullerits, A. Yartsev, V. Sundström, *J. Phys. Chem. Lett.* **2014**, *5*, 2189.
[23] K. Tanaka, T. Takahashi, T. Ban, T. Kondo, K. Uchida, N. Miura, *Solid State Commun.* **2003**, *127*, 619.
[24] Y. Yang, D. P. Ostrowski, R. M. France, K. Zhu, J. van de Lagemaat, J. M. Luther, M. C. Beard, *Nat. Photonics* **2015**, *10*, 53.
[25] A. Miyata, A. Mitioglu, P. Plochocka, O. Portugall, J. T.-W. Wang, S. D. Stranks, H. J. Snaith, R. J. Nicholas, *Nat. Phys.* **2015**, *11*, 582.
[26] Q. Lin, A. Armin, R. C. R. Nagiri, P. L. Burn, P. Meredith, *Nat. Photonics* **2014**, *9*, 106.
[27] K. Zheng, Q. Zhu, M. Abdellah, M. E. Messing, W. Zhang, A. Generalov, Y. Niu, L. Ribaud, S. E. Canton, T. Pullerits, *J. Phys. Chem. Lett.* **2015**, *6*, 2969.
[28] W. Kong, Z. Ye, Z. Qi, B. Zhang, M. Wang, A. Rahimi-Iman, H. Wu, *Phys. Chem. Chem. Phys.* **2015**, *17*, 16405.
[29] C. Wehrenfennig, M. Liu, H. J. Snaith, M. B. Johnston, L. M. Herz, *APL Mater.* **2014**, *2*, 081513.
[30] X. Wu, M. T. Trinh, D. Niesner, H. Zhu, Z. Norman, J. S. Owen, O. Yaffe, B. J. Kudisch, X. Y. Zhu, *J. Am. Chem. Soc.* **2015**, *137*, 2089.
[31] A. Pisoni, J. Jaćimović, O. S. Barišić, M. Spina, R. Gaál, L. Forró, E. Horváth, *J. Phys. Chem. Lett.* **2014**, *5*, 2488.
[32] D. W. de Quilettes, S. M. Vorpahl, S. D. Stranks, H. Nagaoka, G. E. Eperon, M. E. Ziffer, H. J. Snaith, D. S. Ginger, *Science* **2015**, *348*, 683.
[33] M. M. Lee, J. Teuscher, T. Miyasaka, T. N. Murakami, H. J. Snaith, *Science* **2012**, *338*, 643.